AIAA'87

AIAA-87-2108

An Experimental and Numerical Investigation of Swirling Flows in a Rectangular Nozzle

Thomas H. Sobota and Frank E. Marble
California Institute of Technology,
Pasadena, CA

AIAA/SAE/ASME/ASEE 23rd Joint Propulsion Conference

June 29-July 2, 1987/San Diego, California

AN EXPERIMENTAL AND NUMERICAL INVESTIGATION OF SWIRLING FLOWS IN A RECTANGULAR NOZZLE

Thomas H. Sobota†
Frank E. Marble‡

California Institute of Technology
Pasadena, California

Abstract

The high thrust to weight ratios now possible for military aircraft have made thrust vector pitch control more attractive and versatile than aerodynamic surface pitch control. Use of a rectangular nozzle is a natural consequence because articulation and sealing problems are less formidable than for conventional circular nozzles. The rectangular nozzle offers the additional possibility that the exhaust may mix rapidly with the ambient air and thereby reduce the radiative signature of the exhaust. Some previous investigations have suggested that a series of axial vortices may form in the nozzle, as a result of residual swirl from the gas turbine exhaust, and further enhance the mixing rate.

A detailed experimental investigation is described in this paper which demonstrates that the formation of axial vortices in the nozzle is dependant on the vorticity distribution at the turbine exhaust. Further, mechanisms which provide for the formation of axial vortices are identified.

A parallel computational investigation was carried out which not only confirmed the relationship between the turbine exhaust vorticity and the vortex patterns formed in the nozzle but also provided details of the flowfield between the turbine discharge and the nozzle exit. On the basis of this more detailed understanding, it is now possible to "tailor" the vortex distribution at the nozzle exit by design of the turbine discharge and the intervening passage.

Introduction

Recent interest in the use of rectangular nozzles for aircraft application is the primary motivation for this investigation. The next generation of fighter aircraft will require increased maneuverability and STOL (short takeoff and landing) capability. One method for effecting this is through the use of vectored thrust. The rectangular nozzle provides a simple means to vector the thrust about a single axis. The rectangular geometry is being explored as a possibility for aircraft application because vectoring can be accomplished through the use of a relatively simple nozzle design that can also accommodate a variable area ratio convergent–divergent design if such a feature is desired.

Consideration of the thermal characteristics of the exhaust plume is an important aspect of aircraft engine nozzle design. The vulnerability of the aircraft to detection by devices that are sensitive to infrared radiation is directly related to the temperature and extent of the aircraft exhaust plume. In addition to the capability of thrust vectoring, the rectangular nozzle has the additional advantage of a reduced infrared radiation signature. The rectangular geometry of the resulting free jet enhances mixing between the jet fluid and the surrounding ambient fluid. This enhanced mixing serves to dilute the hot combustion products in the exhaust plume with the cold surrounding air. The result is a shorter, cooler exhaust plume. Residual swirl from the turbomachinery in the aircraft engine serves to further complicate the problem. The effect of this swirl and the resulting distribution of vorticity at the exit on the mixing has yet to be examined in detail. Because the distribution of vorticity and pattern of streamwise vortices at the exit will vary greatly with different distributions of velocity at the exit of the engine turbine, there is a need to examine the development of the flowfield within the nozzle for different inlet conditions.

Previous Work

The previous work discussed involves investigations into more basic problems and details pertaining to rectangular nozzles. For the most part, these investigations pertain to the flowfield in the mixing region behind the nozzle. Relatively little work related to the nature of the flowfield within the nozzle has been performed.

Sforza et al. [1] and Sforza and Stasi [2] characterized the mixing field of turbulent rectangular jets into three distinct regions. Near the jet exit is the potential core region characterized by little or no decay of the excess in velocity or temperature along the jet centerline. This is a wedge–shaped region immediately behind the jet exit. The potential core region ends where the two shear layers, which form along the wide edges of the jet, meet. The second region is called the region of characteristic decay because the decay of velocity and temperature along the jet centerline is dependent upon the nozzle geometry or characteristics. The third region is the region of axi-symmetric decay, where the jet characteristics are independent of initial geometry and assume characteris-

†Research Fellow in Mechanical Engineering and Jet Propulsion, Member AIAA

‡Richard L. and Dorothy M. Hayman Professor of Mechanical Engineering and Jet Propulsion, Fellow Member AIAA

tics of the farfield decay of axi–symmetric jets.

Chu et al. [3] undertook an investigation to determine the effect of swirl on the potential core in rectangular ejector nozzles. His water–tunnel tests indicate a dramatic decrease in the length of the potential core region with only small amounts of swirl.

In a water channel flow visualization experiment, Der et al. [4] characterized the evolution of the swirling flow as it passed through a transition section that had a round inlet cross section and a rectangular exit cross section. This was the first attempt to determine, in any detail, the secondary flow patterns at the nozzle exit due to swirl. The apparent splitting of the main swirl into two co–rotating vortices is the most predominant feature of this flowfield. Chu et al. [5][6] attempted to use the results of this investigation to model the infrared signature from a rectangular nozzle, taking into account the effects of swirl in the flowfield. Their findings indicate that the effect of swirl in lowering the plume temperature for a rectangular nozzle is dramatic.

Current Investigation

An understanding of the development of the flowfield within the annular to rectangular transition section as well as the details of the flowfield at the exit would be extremely useful as an aid in designing and predicting the performance of rectangular nozzles. It is postulated that the distribution of axial or streamwise vorticity at the inlet to the transition section will influence, to a large degree, the distribution of vorticity and the formation of streamwise vortex patterns at the exit. This distribution of vortex patterns will significantly affect the nozzle performance as well as the near–field mixing of the exhaust plume. It was the goal of this investigation to determine which features of the inlet vorticity distribution are important in establishing vortex patterns at the exit as well as to examine the evolution of the flowfield as it passes through the transition section. The study of the development of the flowfield will enhance our understanding of the mechanisms by which the vorticity at the inlet is formed into the resulting flow patterns at the exit.

In an attempt to isolate the fluid dynamic phenomena that are important in the development of these flowfields, a controlled investigation was undertaken. A flow configuration that contained the basic characteristics of the original problem was used. These characteristics include an annular inlet cross section, a rectangular exit cross section and a net reduction in the cross–sectional area between the two cross sections. Eliminated from the problem were any features that would serve to unnecessarily complicate the flowfield or make measurement within the flowfield difficult. Features eliminated include any abrupt changes in the cross–sectional area or shape, the flow of hot gases and temperature variation due to combustion, and the effects of compressibility.

Because measurement of the three components of the velocity within the duct would be a difficult and tedious task, an alternate method was desired to determine the development of the flowfield within the duct. There is little other choice than to solve the equations of motion for the entire flowfield within the nozzle. This, of course, must be done numerically with the aid of a computer. Such analysis affords us a knowledge of the flow variables at many points within the nozzle and allows us to follow the development of the flowfield. Therefore, the second part of this investigation entails a detailed modeling of the flow configuration chosen for the experimental investigation.

Experimental Apparatus

Swirling flows in a rectangular nozzle were investigated using the low–speed cold–flow test facility depicted in Figure 1. The contraction section had a cylindrical annular inlet cross section and a rectangular exit cross section. The outer wall in combination with the centerbody was designed to have a smooth monotonically decreasing cross–sectional area. The contraction section had an area ratio of 3.6. The aspect ratio of the rectangular exit was 5.0. Turning blades, stationed at the inlet, were used to introduce swirl into the flow. The turning blades were flat–plate airfoils with no twist constructed of 22 gauge sheetmetal with a pivot attached at the quarter chord point at the root and tip of the blades. A second set of split blades was constructed and was similar in design to the first except that they were separated at the midspan point in such a way that the blade angle could be set independantly for the inner and outer half of the inlet annulus.

Velocity measurements were collected on a rectangular mesh at the exit plane of the contraction section for different inlet conditions. A hot-wire anemometry technique was used to determine the three components of the velocity in the exit plane. The cross-wire probe was mounted in a probe holder which was designed so that measurements could be taken with the sensing elements of the probe in two different orientations. From the four resulting measurements the three velocity components could be determined. The cross–wire probe and probe holder were mounted on a Y–Z traverse. The cross-wire probe was calibrated in a separate calibration duct using the pitot–static probe for the velocity reference. The entire instrumentation system was controlled by a desktop microcomputer.

Experimental Results

To characterize the nature of the flowfield, the velocity at the exit of the contraction was surveyed for three different settings of the inlet turning vanes.

15 Degree Blade Angle and 30 Degree Blade Angle

In this section the two test cases that will be discussed are the result of the same test configuration, only with varying degrees of swirl. The resulting flowfields from these two cases are very similar in some aspects and therefore will be discussed together. The vector plots of

the cross–flow velocity vectors tangent to the exit plane are shown in Figure 2 for the 15 degree swirl case and in Figure 3 for the 30 degree swirl case. The most notable feature here is the strong, concentrated vortex that forms, as expected, along the central axis of the duct. The formation of this vortex can be viewed in any number of ways, the simplest of which is by consideration of the conservation of angular momentum. Due to conservation of angular momentum, the swirl velocity in the neighborhood of the centerbody is increased as the radius of the centerbody decreases. As a result, a strong concentrated vortex is formed along the central axis of the duct.

Perhaps a more informative way to look at this vortex formation is through vorticity considerations. The axial vorticity in the boundary layer along the centerbody is affected in two ways. First, this vorticity is convected downstream along the centerbody so as to form one vortex tube along the central axis of the duct. Second, because the flow is accelerated by contraction of the channel, the vortex strength increases through vortex stretching.

The second predominant feature of these two cases is the two vortices which are formed anti–symmetrically about the central vortex. While these vortices are present for both the low and high swirl cases, they are much stronger and more developed in the high swirl case. These vortices are of opposite sense to the swirl introduced at the inlet. At the inlet, a boundary layer forms on the outer wall which contains vorticity of this opposite sense. The vorticity in these vortices can be attributed to these boundary layers, which are shed from the wall and then entrained into the main stream.

Split Blades

Earlier work by Der et al. [4] indicates the formation of two co–rotating streamwise vortices at the exit of a similar flow configuration. It became apparent that, because these flows are convection dominated, in order to get vorticity in the center of the stream it would be necessary to introduce vorticity somewhere midspan at the inlet section. This was effected by using turning vanes at the inlet, which were constructed in such a way that the blade angle for the inner and outer half of the annular inlet section could be set independently. Using these blades, one experimental case was examined. For this set of measurements the blade angle for the inner half of the annulus was set to 0 degrees and the blade angle for the outer half was set to 30 degrees.

Figure 4 is the cross–flow velocity vector plot measured at the exit plane. One can see the formation of two streamwise vortices. The vortex sheet formed midspan at the inlet is convected downstream to the exit plane. The resulting distribution of vorticity is such that the induced cross–flow velocities give rise to two regions of swirling fluid. Additionally, two smaller vortices in the diagonally opposed upper left and lower right hand corners are formed. These are a result of the boundary layer which forms on the outer wall of the duct separating from the wall in the neighborhood of these corners.

Numerical Investigation

The numerical analysis was performed for two distinct purposes. First, it allowed examination of the detailed development of the flowfield between the blade row discharge and the nozzle discharge. These details were not generally available for measurement. Second, once confidence is developed in accuracy of the computational result, it provides a means to examine the discharge flows resulting from more complex blade row configurations. In this section we will discuss the numerical approach used to examine this flowfield and then examine the results of some of the numerical cases which were run.

Numerical Model

The flowfield was computed using the INS3D computer code developed by Kwak et al. [7]. The algorithm used was an implicit finite difference code, which solves the incompressible Navier–Stokes equations in a generalized curvilinear coordinate system. The method of pseudocompressibility originally proposed by Chorin [8] was used to facilitate the solution to the pressure field. The resulting equations were approximately factored using the technique proposed by Beam and Warming [9]. For more detailed information reference should be made to references 7, 10, 11, and 12. Additionally a detailed account of the application of this code to the current problem is provided in reference 13.

Turbulence modeling for high Reynolds number flows is the subject of much current investigation. Internal flows and regions of separation prove to be particularly difficult to model. Because of the difficulty of computing high Reynolds number flows, the laminar steady Navier–Stokes Equations were solved instead of attempting to solve the Reynolds averaged equations with the use of a turbulence model. The flows investigated numerically were computed with a Reynolds number of 4500 based on the height of the exit cross section. For the purpose of comparison, the Reynolds number for the experimentally determined flowfields was approximately 30,000. The use of the steady laminar Navier–Stokes equations in order to obtain a description of the flowfield, which compares well in a qualitative sense with the experimental results, is deemed adequate so long as the Reynolds number used to compute the flows is high enough so that the flow is momentum dominated. If this is the case, the boundary layer growth is small and confined to a region near the walls and therefore the gross characteristics of the flowfield are independent of the Reynolds number. The Reynolds number of 4500 was chosen for the computation so that the boundary layer thickness at the exit for the computed flows was approximately the same as the exit boundary layer thickness measured in the experiment.

Computational Grid

The computer code INS3D requires a surface– conforming computational grid. At the current time, general three–dimensional grid generation programs are not

readily available. The three–dimensional grid for the current investigation was generated by creating a set of two–dimensional grids for a number of subsequent axial locations and then stacking these grids to form the desired three–dimensional mesh. A uniform mesh spacing in the axial direction was used. For each planar axial station, the grid was generated using the GRAPE computer code developed by Sorenson [14]. Figure 5 shows one quarter of the outer boundary as well as the exit plane. It should be noted here that the shape of the centerbody was altered for the purpose of the numerical investigation. It was anticipated that the blunt end of the centerbody would cause numerical difficulty and was eliminated in favor of a conical tip on the downstream end of the centerbody. The shape of the outer boundary was also changed so that the cross–sectional area of the flow system would increase monotonically and vary smoothly.

Numerical Results

The computer code INS3D was used to model the flow in the experimental flow configuration for two different inlet conditions. For the purpose of comparison with the experimental results, the results of the computation at the exit plane were interpolated from the the computational grid onto the mesh used in the experiment for the 15 degree swirl case and for the split blade case. The cross–flow velocity vector plots for these two cases are shown in Figures 6 and 7, respectively. A comparison of these plots with the experimental results indicates good agreement between the computational and experimental results.

Discussion

Presentation of the Results

The results of the computation will be presented on planar cross–sectional cuts perpendicular to the axial direction, which is also the primary flow axis. Some of the features of the flowfield of current interest evolve slowly in the axial or streamwise direction. In this case, it is informative to view several successive cross–sectional cuts of the flowfield. Cross–flow velocity vector plots and vorticity contour maps will be presented in this way. The view will be in the upstream direction as in Section A–A on Figure 8. Because all of the flows to be discussed are antisymmetric about the duct center, it is sufficient to display only one half of the cross–sectional cut. The half depicted in the plots to follow will be the half from just left of the center to the right edge. A station number will indicate the axial position of the cross section depicted. Figure 8 also provides the location of the station numbers. On the contour plots, contours of positive vorticity will be represented by solid lines, contours of negative vorticity will be represented by dashed lines, and the zero vorticity contours will be shown as dotted lines.

15 Degree Blade Angle and 30 Degree Blade Angle

Before we look at the flowfields that result from these configurations, it would be informative to know where and how vorticity is introduced into the flowfield. In order to determine which features of the inlet vorticity field are important in the formation of vortex patterns at the exit of the transition section, it is necessary to characterize the inlet flowfield produced by the turning vanes. Here we examine the flowfield some small distance downstream of the turning vane assembly, where we have an annular flow cross section formed by two concentric cylinders and therefore adopt a cylindrical coordinate system for the inlet. Recall that the turning vanes are flat plate airfoils with no twist. Assuming that the fluid leaves the turning vane assembly parallel to the blades, the tangential component (w) of the velocity is proportional to the axial component (u).

$$w = u \tan\theta,$$

where θ is the angle between the turning vane and the duct axis. We assume that any resulting radial component (v) is small and will be neglected for the purpose of this discussion. The assumption that the fluid leaves the turning vane assembly parallel to the blades was verified, using a simple tuft flow visualization. In this cylindrical coordinate system the three vorticity components, ς, ξ, and η in the axial (x), radial (r), and tangential (ϕ) directions, respectively, can be written:

$$\varsigma = \frac{\delta w}{\delta r} + \frac{w}{r} - \frac{1}{r}\frac{\delta v}{\delta \phi}$$

$$\eta = \frac{\delta v}{\delta x} - \frac{\delta u}{\delta r}$$

$$\xi = \frac{1}{r}\frac{\delta u}{\delta \phi} - \frac{\delta w}{\delta x}.$$

In the flowfield, away from the walls so that the effects of the boundary layers are not significant, the vorticity components reduce to:

$$\varsigma = \frac{u \tan\theta}{r}$$

$$\xi = 0$$

$$\eta = 0.$$

This vorticity shed from the turning blade is due to a variation in lift along the span of the blade. Therefore, it should be recognized that the above description of the flowfield is an idealization of the flowfield that actually develops. In the actual flowfield, the vorticity is present only in the wake of the airfoils. In this description we have distributed the vorticity uniformly in the tangential direction. We will see later that this idealization has little effect on how we view the results.

Because of its importance in the downstream vortex patterns, it is also necessary to examine the axial vorticity that is contained in the boundary layers on the outer wall of the flow passage and on the centerbody. In fact, this vorticity dominates the flowfield. If we examine a cross–sectional cut of the inlet section in a plane perpen-

dicular to the axial flow direction, we have a tangential velocity profile that is represented, approximately, in Figure 10a. Here we assume that there is a region away from the wall that is unaffected by the formation of the boundary layers and behaves as described above. Because of the no–slip condition, which must be imposed at the walls, the flowfield near the walls must deviate from the uniform tangential velocity profile in order to accommodate zero velocity at the wall. The axial vorticity profile resulting from the velocity profile in Figure 10a is depicted in Figure 10b.

From this figure it can be seen that the level of vorticity in the region away from the wall is small compared to the levels in the boundary layer, and for the purpose of this discussion, the flow away from the wall will be considered to be irrotational. The vorticity level in the region away from the wall is low enough with the flat blades that it can be neglected in initial attempts to characterize the flow. As in any high Reynolds number flow, the boundary layers formed remain thin and, in the absence of separation, these boundary layers and the vorticity associated with them remain adjacent to the wall.

As stated earlier, the predominant feature at the exit plane in the low swirl case is the formation of a strong, streamwise vortex along the central axis of the duct. Figure 10b shows the vorticity profile at the inlet just downstream of the turning vanes. In the neighborhood of the centerbody, at the blade root, the axial vorticity is high and positive in sense. This vorticity is convected toward the downstream tip of the centerbody and then along the central axis of the duct downstream of the centerbody. This convective process forms a core of axial vorticity along the central axis. This vorticity is subsequently stretched as the fluid is accelerated through the remainder of the contraction section and is apparent as a strong, streamwise vortex at the exit plane.

In the cross–flow velocity plots at the exit plane for the low swirl case, two streamwise vortices located antisymmetrically about the central vortex are visible. As stated earlier, these vortices are the result of the separation of the outer boundary layer into the main stream. The cross–flow velocity vector plots and the vorticity contour plots for a series of axial stations upstream of the exit plane are presented in Figures 9a-c. From these plots the growth of the separated region can be traced as it evolves in the axial direction.

In the experimental cross–flow velocity vector plots for the high swirl case, Figure 3, this pair of axial vortices is also apparent. Unfortunately, results of the numerical computation are not available for the high swirl case. However, in light of the results of the computation for the low swirl case and the experimental results for the high swirl case, the author has some confidence in his speculation on the differences between these two cases. In the high swirl case, the pair of axial vortices are much larger and move nearly to the center of the duct cross section. This occurs for two reasons. First, because the cross–flow velocities are much larger and the resulting cross–flow pressure gradient much stronger in the high swirl case, the separated region forms further upstream. The increased length of this separation line allows for a separation of a greater percentage of the boundary layer fluid. The second reason for the increased strength of the vortices shed from the wall is simply due to the fact that the net quantity of axial vorticity (axial vorticity integrated over the cross section of the boundary layer) is greater for the high swirl case than for the low swirl case. In fact, if we maintain that the fluid that originated at the inlet outside of the boundary layer is still irrotational at the exit, then the net vorticity in the boundary layer is equal in magnitude to the circulation around the central vortex.

The fact that the vorticity in the vortex pair that is shed from the wall must have its origin in the boundary layers on the outer wall shows that there is a maximum for the strength of these shed vortices. A measure of the strength of these vortices is the circulation taken on a contour in a plane of constant X, that surrounds the center of the vortex. The maximum strength of each of these vortices is then equal to one half of the circulation taken on a contour that surrounds only the central vortex.

These qualitative observations may be given some substance by examining circulation integrals about certain regions at the exit plane. The circulation is defined as:

$$\Gamma = \oint \vec{V} \cdot \vec{dl}$$

and is normalized by the circulation introduced upstream by the blade row. For the high swirl case the nondimensional circulation along a contour that includes only the central vortex is approximately 0.75, whereas the circulation around a contour surrounding the entire flowfield is two orders of magnitude lower. The circulation about each of the two shed vortices is approximately -0.3. This indicates that most of the vorticity and hence most of the fluid initially in the boundary layer along the outer wall has been entrained into the main stream. In choosing the contours of integration, some effort was made to maximize the result of the numerical integration.

Split Blades

Again, to assess which characteristics of the inlet flowfield are important in the downstream vortex pattern formation, it is necessary to examine the inlet flowfield in some detail. An approximate representation of the tangential velocity just downstream of the inlet turning vanes is depicted in Figure 11a. In this case, the tangential velocity is zero for the inner half of the annulus and, as in the case above, the tangential velocity for the outer half is $U \tan \theta$. The resulting vorticity profile is depicted in Figure 11b. Here again, the vorticity shed along the span of the blade due to the variation in lift along the blade in the outer half of the inlet annulus is small compared to the vorticity in the boundary layer at the outer wall and the vorticity shed as tip vortices from the free end of the turning blades. Therefore, the effect of spanwise lift variation in the outer region will be neglected in this discussion. We have, in effect, introduced a cylindrical sheet of axial vorticity midspan in the inlet section.

Again, it should be noted that to consider this to be a sheet of vorticity evenly distributed in the tangential direction is an idealization of the actual flow in which the vorticity is introduced midspan as a series of streamwise axial vortices, one shed from each of the tips of the turning vanes. It can be argued that these tip vortices are spread in the tangential direction by the radial gradient of the tangential velocity.

Again, in this case it is informative to trace the flowfield development by examining the cross-flow velocity and the axial vorticity contours on a series of subsequent cross-sectional cuts of the flowfield. The cross-flow velocity vector plots and the corresponding axial vorticity contours in Figures 12a-d trace the development of the flowfield from a cross section near the inlet to the exit plane.

The cross-flow velocity vector plot at the exit plane (Figure 12d) shows the formation of a streamwise vortex or region of swirling flow. An examination of the corresponding vorticity contour plot shows a large area of positive axial vorticity in this region, with no strong peak in the axial vorticity magnitude. By examining the evolution of this flowfield, starting with a cylindrical vortex sheet at the entrance, one can trace the development of this sheet as it is convected downstream. The shape of this sheet is distorted as the shape of the inner and outer flow boundary change. The sheet tends to roll up, or at least, vorticity tends to accumulate in the region where the sheet is most distorted. This results in a swirling flow in this region. As mentioned earlier, there is no sharp peak in the axial vorticity magnitude in this region, but instead, a relatively large area that contains positive axial vorticity. The velocities induced by this region tend to re-entrain the rotational fluid originally in the shear layer as well as a portion of the irrotational fluid from the central region of the flow. As a result, we get a broad region of positive axial vorticity.

Also worth noting are the two small streamwise vortices, one of which forms in the lower right-hand corner of the rectangular exit cross section, and the other in the diagonally opposed corner. These are due to the separation of the boundary layer that forms on the outer wall.

Conclusions

A controlled investigation was undertaken to determine the effects of swirl on the flowfield that develops in an annular to rectangular transition section. The flow patterns at the exit were found to depend strongly on the distribution of axial vorticity at the annular inlet. The use of a steady laminar incompressible Navier-Stokes algorithm on a digital computer was found to adequately model the qualitative features of the flowfield.

In the low and high swirl cases the majority of the vorticity was introduced in the neighborhood of the blade root and the blade tip in the boundary layers on the centerbody and outer wall, respectively. The axial vorticity introduced at the blade root was convected along the centerbody to the downstream tip and then along the centerline of the transition section. This resulted in the formation of a strong vortex along the central axis of the duct. The pressure gradient established on the outer wall of the duct, as a result of the strong central vortex, promoted the separation of the boundary layer from the outer wall into the main stream. This separation was evident in the formation of two streamwise vortices, one on each side of the central vortex, which had a sense opposite to the sense of the central vortex. This effect was much more pronounced in the high swirl case, as the pair of vortices formed was much stronger and moved nearly to the center of the height of the rectangular exit. It was argued that the maximum strength of these two vortices could be related to the strength of the central vortex and that the maximum strength was nearly achieved in the high swirl case.

In another test case, a set of blades that introduced swirl into only the outer half of the inlet annulus was used. This, in effect, introduced a cylindrical sheet of streamwise vorticity into the flow at the inlet at a radial position halfway between the centerbody and the outer wall. There was also axial vorticity of the opposite sense introduced into the boundary layer on the outer wall. In this case the separation of the boundary layer on the outer wall did not occur to a significant extent but was apparent in the formation of two small, streamwise vortices in diagonally opposed corners of the rectangular exit cross section. The cylindrical vortex sheet, when convected through the annular to rectangular transition section, was distorted in such a way as to conform to the shape of the outer wall of the duct. In the regions where the vortex sheet was most distorted, it tended to roll up. The result was the formation of two axial streamwise vortices at the exit plane of the duct.

The effect of swirl on the nearfield mixing of the jet issuing from the rectangular nozzle was not investigated. However, an examination of the vortex patterns leads one to conjecture on the relative effectiveness of these patterns in enhancing the nearfield mixing. The no swirl case is of little practical interest for two reasons. First, the features of the geometry that caused the formation of the four streamwise vortices are not present in the practical problem. Second, the strength of these vortices was very small and their effect on the mixing of the plume will, in all likelihood, be negligible.

The two axial vortices formed when swirl was introduced into only the outer half of the inlet annulus will, in all likelihood, enhance the nearfield mixing of the resulting jet. The combination of shear in the direction normal to the direction in which the jet forms and possibly an increase in large-scale entrainment due to the vortex pattern would serve to reduce the potential core size.

The vortex patterns created in the low and high swirl cases appear to be highly conducive to the mixing of the rectangular jet, particularly in the high swirl case. The adjacent positioning of strong vortices of opposite sense will tend to draw the cold ambient fluid between them. This large-scale mixing will rapidly reduce the size of the potential core region of the jet.

The discussion above, pertaining to mixing of the rectangular jet, is conjecture based on observation of the the flow patterns at the exit of the transition section. In order to accurately determine the mixing field in the region immediately behind the nozzle exit, it is suggested that a separate investigation be undertaken.

If it is the nozzle designer's intent to create a flowfield that enhances mixing, he is, of course, not limited to the vorticity distributions examined in this investigation. The possibility of varying the vorticity distribution at the annular inlet to the transition section for the purpose of tailoring the vortex pattern at the exit is worth consideration. The distribution of axial vorticity at the inlet could be varied not only in the radial direction, but also in the tangential direction. A non–axi–symmetric distribution of vorticity at the inlet could be used to place vorticity and encourage the formation of axial vortices at any location in the exit. The other possibility for tailoring the flowfield involves contouring the duct shape so as to promote either the separation of the boundary layers on the outer wall or the formation of streamwise vortices from vorticity distributed throughout the flow. The current investigation provides an understanding of the mechanisms by which the streamwise vortices are formed. This understanding is valuable in any effort to tailor the flow, whatever the intended purpose.

References

[1] Sforza, P. M., Steiger, M. H., and Trentacoste, N., "Studies on Three–Dimensional Viscous Jets," *AIAA Journal*, vol. 4, no. 5, pp. 800–806, 1966.

[2] Sforza, P. M. and Stasi, W., "Heated Three–Dimensional Turbulent Jets," *Journal of Heat Transfer*, vol. 101, no. 2, pp. 353–358, 1979.

[3] Chu, C., Der Jr., J., Ortiz, V. M., and Widynski, T. C., "Effect of Swirl on the Potential Core of Two–Dimensional Ejector Nozzles," *Journal of Aircraft*, pp. 191–192, February 1983.

[4] Der Jr., J., Chu, C., Hunt, B. L., and Lorincz, D. J., "Evolution of Swirl in a Two–Dimensional–Nozzle Flow," *Journal of Aircraft*, vol. 19, pp. 347–349, April 1982.

[5] Chu, C., Der Jr., J., and Wun, W., "A Simple 2D Nozzle Plume for IR Analysis," in *AIAA Aircraft Systems Meeting*, August 1980., AIAA–80-1808.

[6] Chu, C. and Der Jr., J., "Modeling of 2D Nozzle Plume for IR Signature Predictions Under Static Conditions," in *AIAA Aircraft Systems Meeting*, August 1980., AIAA–80-1808.

[7] Kwak, D., Chang, J. L. C., Shanks, S. P., and Chakravarthy, S. R., "An Incompressible Navier–Stokes Flow Solver in Three–Dimensional Curvilinear Coordinate System Using Primitive Variables," in *AIAA 22th Aerospace Sciences Meeting*, January 1984., AIAA–84-0253.

[8] Chorin, A. J., "A Numerical Method for Solving Incompressible Viscous Flow Problems," *Journal of Computational Physics*, vol. 2, pp. 12–26, 1967.

[9] Beam, R. M. and Warming, R. F., "An Implicit Finite Difference Algorithm For Hyperbolic Systems in Conservation Law Form," *Journal of Computational Physics*, vol. 22, pp. 87–110, September 1976.

[10] Chang, J. L. C., Kwak, D., Dao, S. C., and Rosen, R., "A Three–Dimensional Incompressible Flow Simulation Method and its Application to the Space Shuttle Main Engine, Part I — Laminar Flow," in *AIAA 23rd Aerospace Sciences Meeting*, January 1985., AIAA–85-0175.

[11] Chang, J. L. C., Kwak, D., Dao, S. C., and Rosen, R., "A Three–Dimensional Incompressible Flow Simulation Method and its Application to the Space Shuttle Main Engine, Part II — Turbulent Flow," in *AIAA 18th Fluid Dynamics and Plasmadynamics and Laser Conference*, July 1985., AIAA–85–1670.

[12] Chang, J. L. C. and Kwak, D., "On the Method of Pseudo Compressibility for Numerically Solving Incompressible Flows," in *AIAA 22nd Aerospace Sciences Meeting*, January 1984., AIAA–84-0252.

[13] Sobota, T. H., *An Experimental and Numerical Investigation of Swirling Flows in a Rectangular Nozzle.*, PhD Thesis, California Institute of Technology, Pasadena, California, 1987.

[14] Sorenson, R. L., "A Computer Program To Generate Two-dimensional Grids About Airfoils and Other Shapes By the Use of Poisson's Equation," Tech. Rep. NASA TM-81198, 1981.

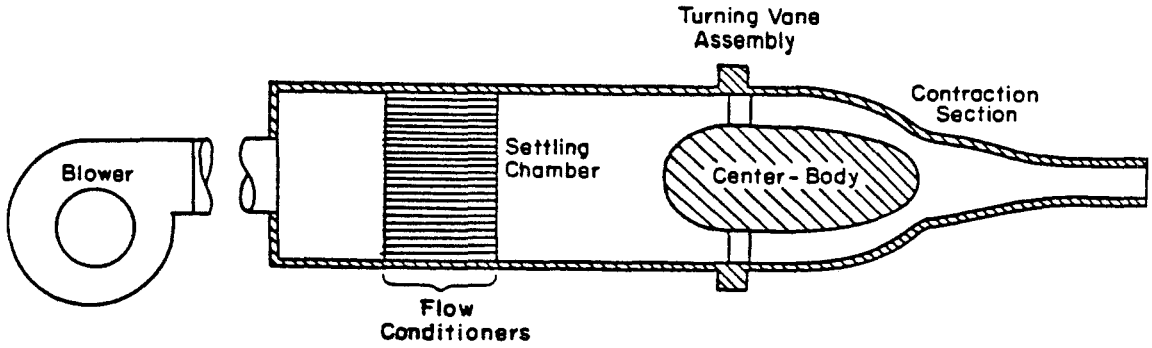

Figure 1: Schematic Diagram of the Flow System

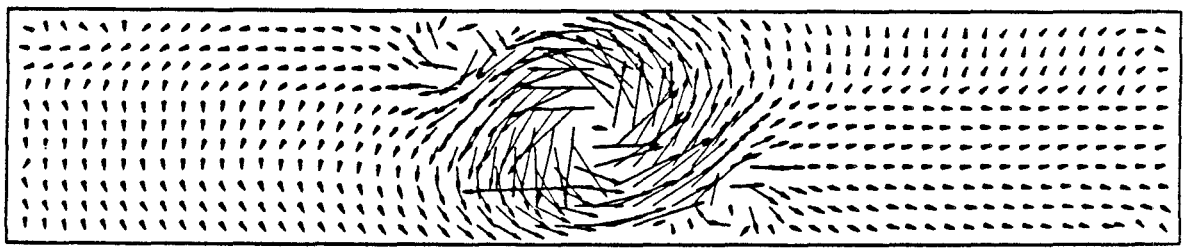

Figure 2: Cross-Flow Velocity Vector Plot, 15 Degree Blade Angle (Measured)

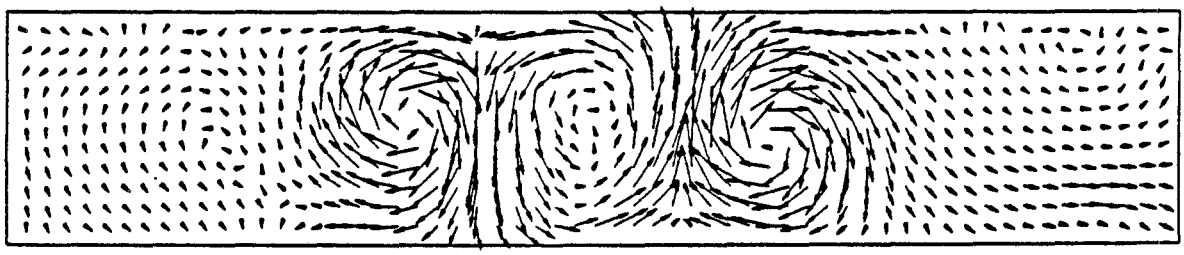

Figure 3: Cross-Flow Velocity Vector Plot, 30 Degree Blade Angle (Measured)

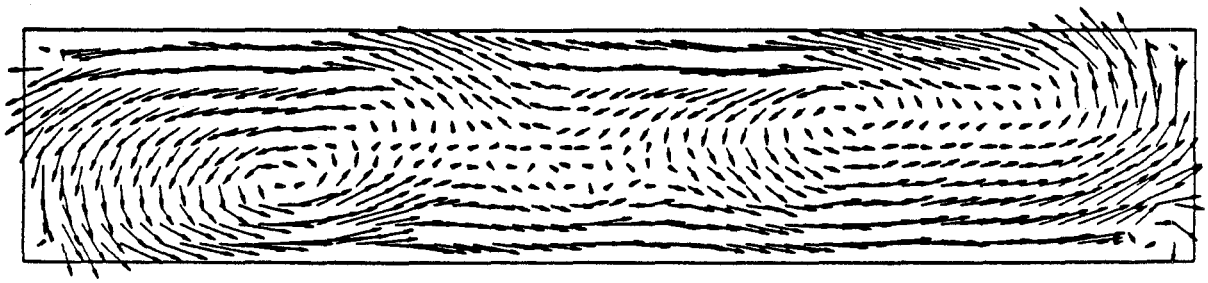

Figure 4: Cross-Flow Velocity Vector Plot, Split Blades (Measured)

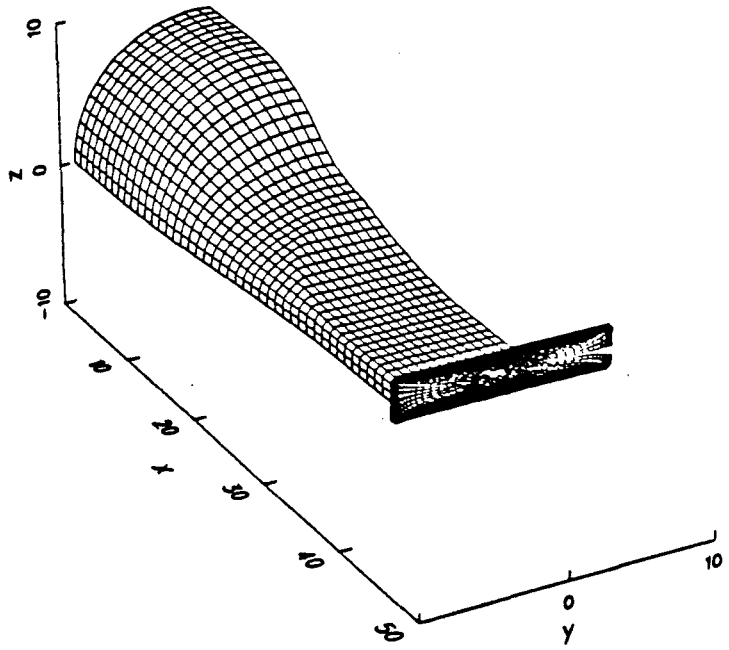

Figure 5: Outer Surface and Exit Plane of Computational Grid

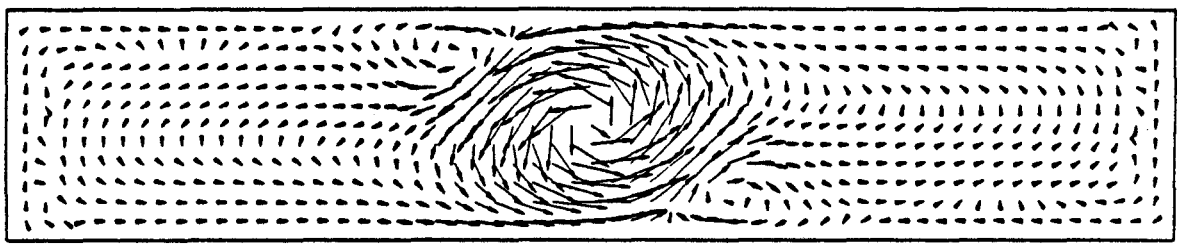

Figure 6: Cross-Flow Velocity Vector Plot, 15 Degree Blade Angle (Computed)

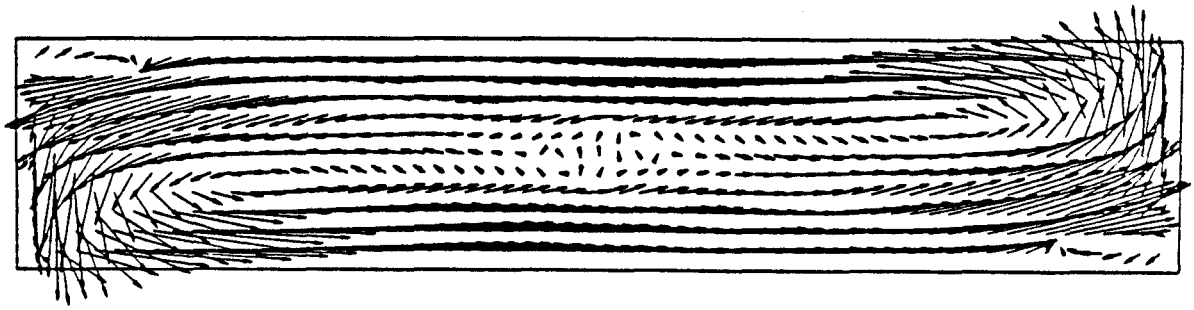

Figure 7: Cross-Flow Velocity Vector Plot, Split Blades (Computed)

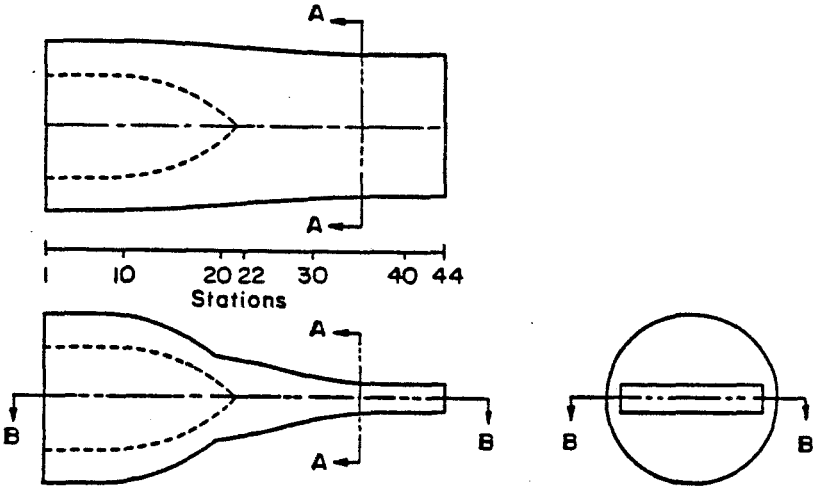

Figure 8: Sections and Stations

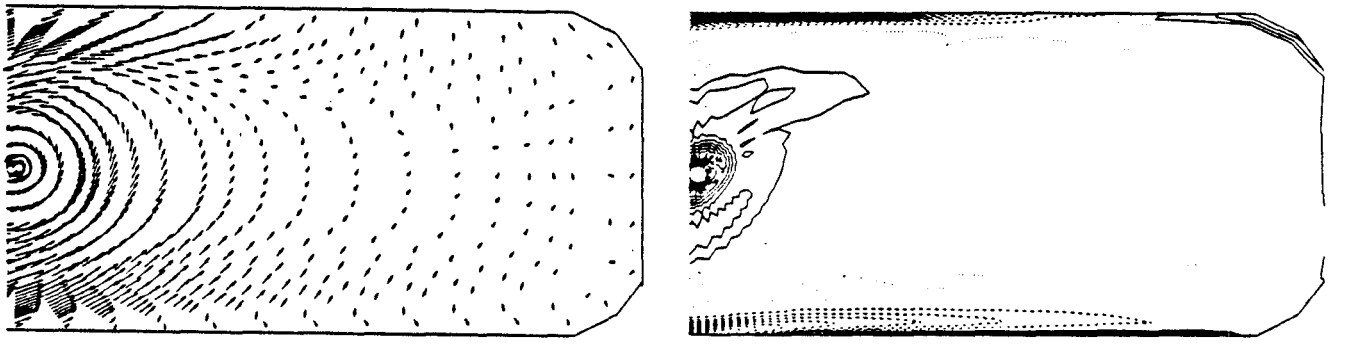

a) Station 32

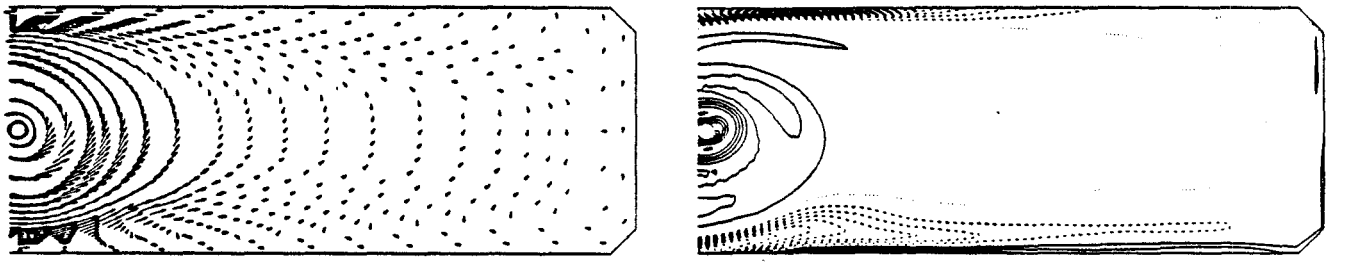

b) Station 38

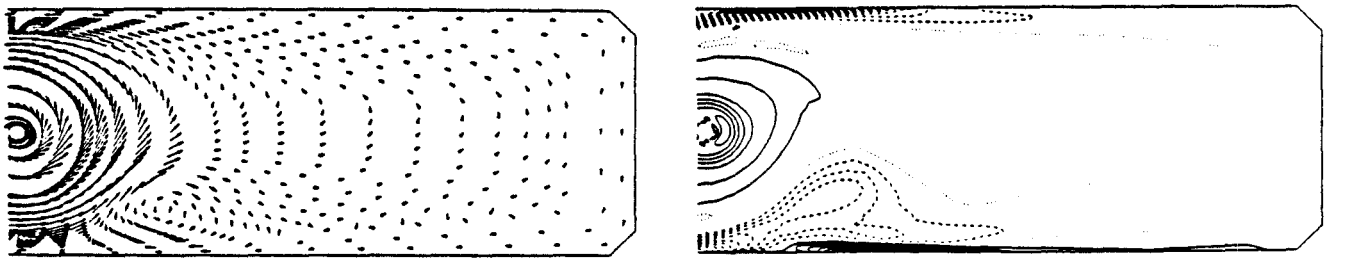

c) Station 44

Figure 9: Cross-Flow Velocity Vector Plots and Axial Vorticity Contour Plots, 15 Degree Blade Angle

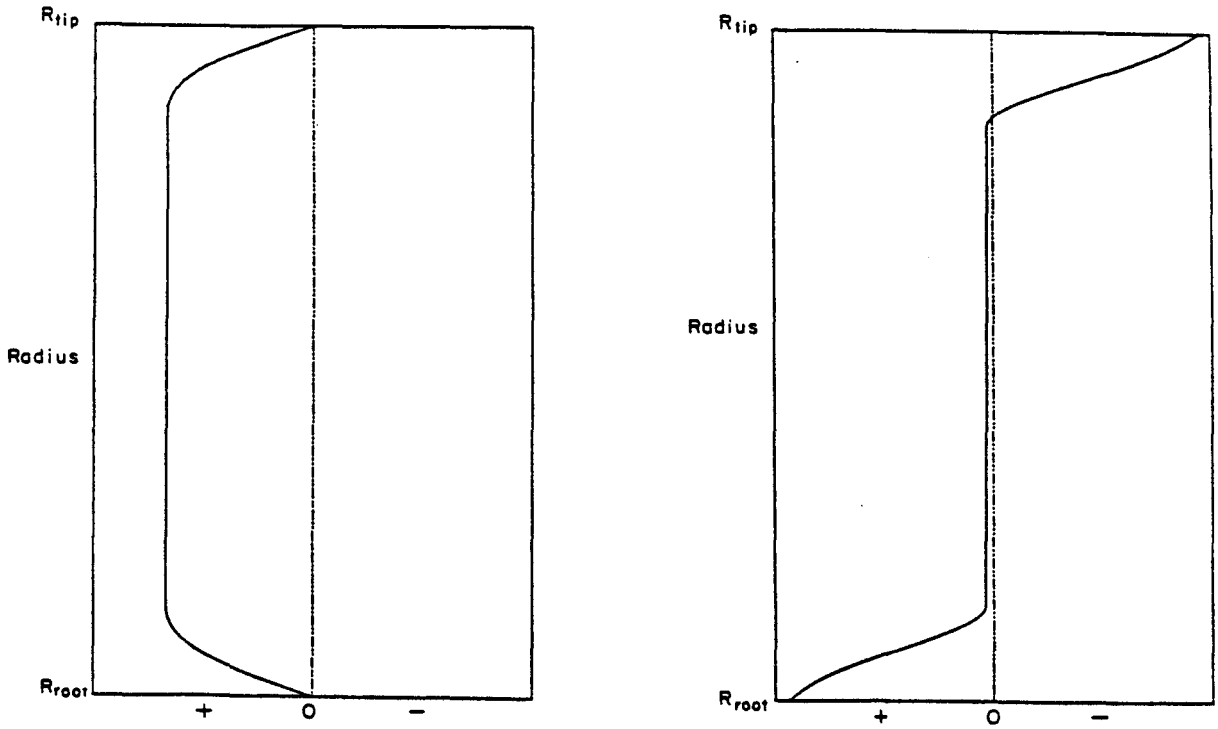

a) Tangential Velocity

b) Axial Vorticity

Figure 10: Inlet Conditions, 15 Degree Blade Angle

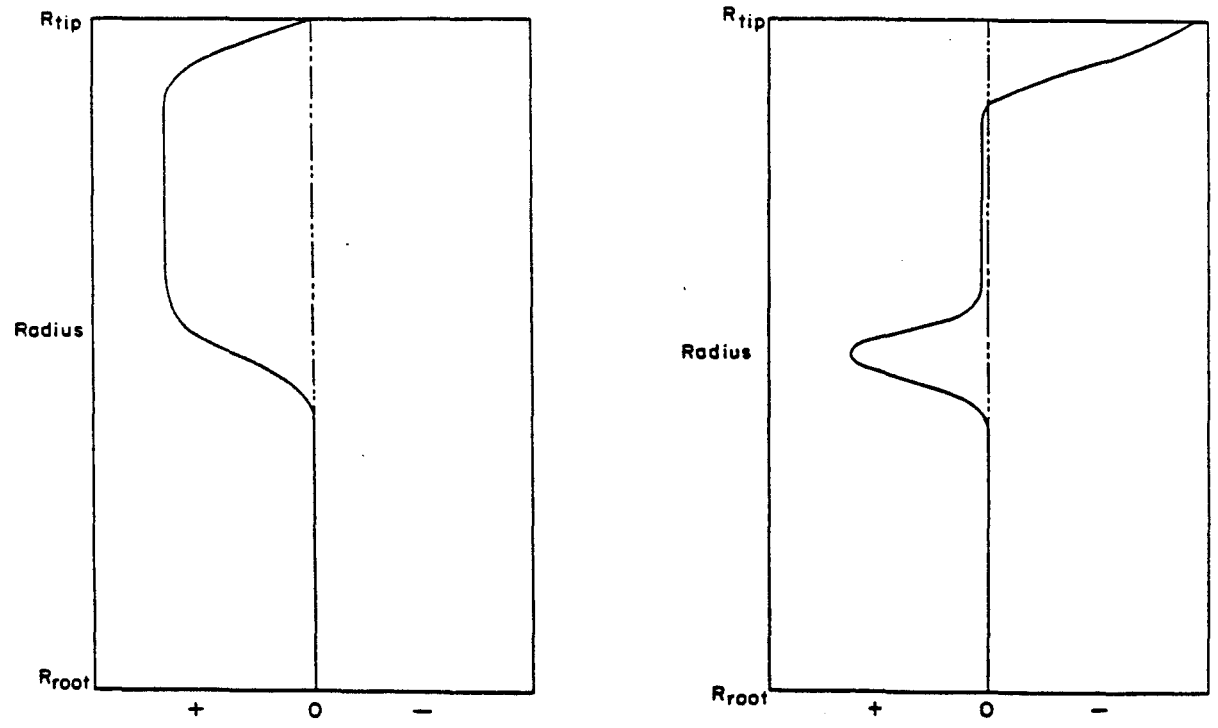

a) Tangential Velocity

b) Axial Vorticity

Figure 11: Inlet Conditions, Split Blades

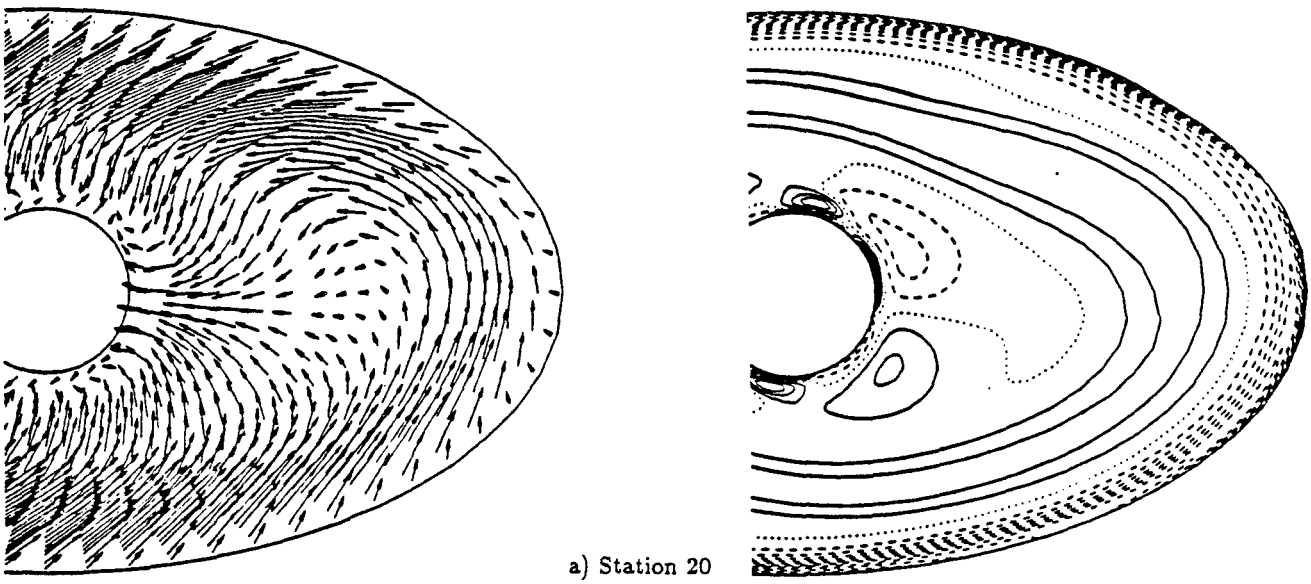

a) Station 20

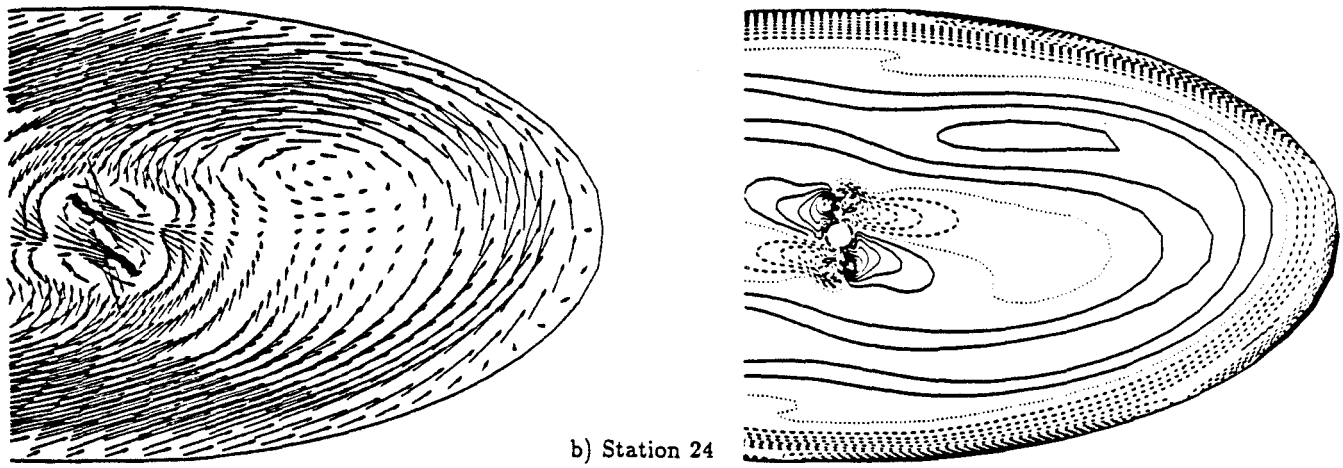

b) Station 24

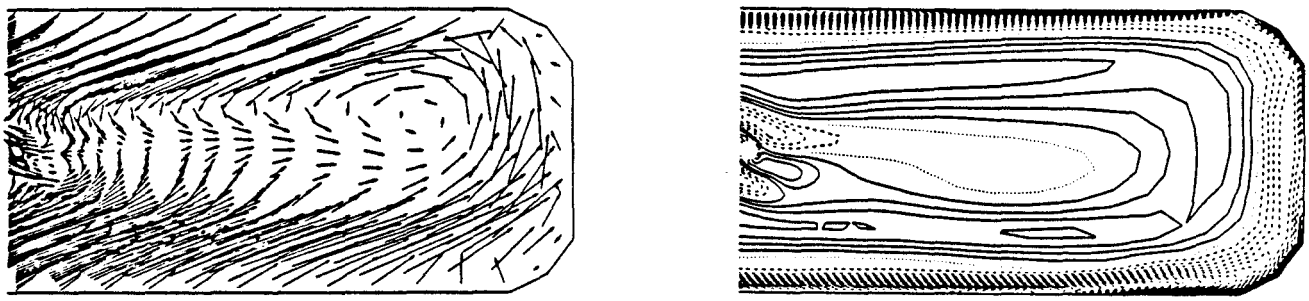

c) Station 32

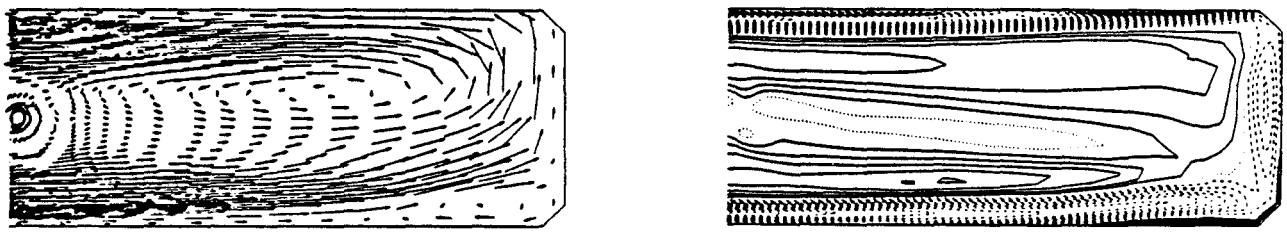

d) Station 44

Figure 12: Cross-Flow Velocity Vector Plots and Axial Vorticity Contour Plots, Split Blades